Exhaust Thermal Management in a Dual-Fuel Marine Engine via Fully Variable Valve Actuation and Wastegate Lambda Control

SAE Technical Paper 2025-24-0085, 2025, doi:10.4271/2025-24-0085

Exhaust thermal management in a dual-fuel marine engine via fully variable valve actuation and wastegate lambda control

Amir Soleimani[1)], Jeyoung Kim[1)], Martin Axelsson[2)], Jari Hyvonen[2)] , Maciej Mikulski[1)]
[1)] University of Vaasa, School of Technology and Innovation, Efficient Powertrain Solutions (EPS) research group, Wolffintie 34, FI-65200 Vaasa, Finland
[2)] Wärtsilä Finland Oy, Frilundintie 7, FI-65170 Vaasa, Finland

Abstract
Dual-fuel combustion is emerging as a promising solution to address the growing focus on maritime decarbonization, because it is adaptable and needs minimal system modifications. However, natural gas as an alternative fuel must deal with the issue of methane slip, because methane has greater global warming potential than CO2. Conventional aftertreatment systems may incorporate a methane oxidation catalyst to mitigate methane emissions, but effective methane oxidation requires high temperatures of approximately 400 °C. Therefore, exhaust thermal management (ETM) is crucial for maintaining high exhaust gas temperature (EGT) and ensuring conversion efficiency. This study investigates the effectiveness of fully variable valve actuation (VVA), including early exhaust valve opening (EEVO) and early intake valve closing (EIVC), along with lambda control via wastegate control. Each strategy's effect on exhaust gas temperature is evaluated, while considering potential trade-offs with efficiency. The research uses a model-based approach, simulating a state-of-the-art, six-cylinder natural gas/diesel dual-fuel marine engine (Wärtsilä 6L20 DF), equipped with a two-stage turbocharger with wastegates. Numerical simulations are conducted using a one-dimensional (1D) engine model within GT-Suite across two different load conditions. The model is validated using baseline valve timings and a comprehensive dataset of experimental data. Results indicate that all three strategies can contribute to EGT elevation. EEVO raises EGT by 73 K, but incurs a 3.85% reduction in brake thermal efficiency (BTE). EIVC achieves a substantial EGT increase of 122.7 K at medium load, with a slight BTE improvement of 0.4%. Wastegate lambda control elevates EGT by 91.5 K at low load, exhibiting a negligible BTE impact. Thus, VVA-based ETM and lambda control enable rapid warm-up of exhaust aftertreatment systems (EATS) in large-bore engines with a minor efficiency penalty. This helps compliance with stricter emission regulations which contribute to maritime decarbonization, eventually enhancing air quality and the maritime ecosystem.

Introduction
The marine propulsion sector has been steadily evolving towards decarbonization, supported by the greenhouse gas (GHG) reduction strategy introduced in 2018 by the International Maritime Organization (IMO) [1]. The strategy has recently been tightened towards achieving net-zero GHG emissions by 2050, through the adoption of low-carbon fuels, and clean energy sources [2].
Dual-fuel (DF) engines operating on natural gas (NG) and diesel, encompassing both conventional and reactivity-controlled compression ignition (RCCI) combustion, have gradually been replacing legacy diesel propulsion in recent years. DF engines are advantageous for reducing CO_2 emissions because natural gas (NG) has a more favorable hydrogen-to-carbon ratio than diesel. However, methane slip - the exhaust emission of unoxidized CH_4 - remains a critical issue [3]. Methane (CH_4) has a significantly greater global warming potential (GWP) than carbon dioxide (CO_2) on a 20-year timescale (GWP_{20}=81.1) [4]. Consequently, even a small amount of methane slip can offset the carbon emission benefits of switching to NG.

Methane slip in natural-gas dual-fuel engines stems chiefly from four mechanisms: (i) incomplete combustion when an excessively lean premixed charge cannot sustain flame propagation, a condition exacerbated at low loads and transient operation [5]; (ii) wall-quenching, where rapid heat loss to cooler cylinder surfaces extinguishes the flame, a phenomenon that is the main contributor at low loads [5]; (iii) crevice trapping, in which narrow piston-ring, gasket and liner clearances shield pockets of methane from the flame front, releasing them unburned during the exhaust stroke [6]; and (iv) scavenging, whereby valve-overlap allows part of the fresh methane-air mixture to bypass the combustion chamber and escape directly to the exhaust [7].

Some researchers have focused on reducing methane slip at its source, by, for example, reducing crevice volumes through optimized combustion chamber geometry [8], [9], [10]. Additionally, enhancing air-fuel mixing can improve combustion completeness [11]. But even these strategies leave some residual methane, so contemporary studies recommend combining them with lean-compatible aftertreatments, especially methane-oxidation catalysts (MOCs) which can approach complete conversion. However, the high chemical stability of methane means a relatively high reaction temperature is required to break its strong C–H bonds. Catalysts, particularly those based on palladium (Pd), have shown promising results for complete methane oxidation [12]. Unfortunately, Pd-based catalysts are highly susceptible to sulfur poisoning and deactivation by water vapor [13], [14], [15]. Even trace amounts of sulfur dioxide (SO_2), as little as 1 ppm, can severely inhibit catalyst performance [16], [17]. Technologies for efficient regeneration or mitigation of SO_2 exposure are therefore critical for the commercial implementation of MOCs.

Several regeneration strategies have been investigated. Honkanen et al. [11] used methane-rich conditions to regenerate sulfur-poisoned Pd catalysts. Kinnunen et al. [18] demonstrated regeneration under low-oxygen conditions, while Heikkilä et al. [19] and Jones et al. [20] employed hydrogen to restore catalyst activity.

The sulfur content in fuel and lubricants must be limited to minimize SO_2 in the exhaust. NG typically contains only a few ppm of sulfur. The pilot diesel fuel, though regulated to a sulfur content of 0.5% globally and 0.1% within Emission Control Areas (ECA) by the IMO, still contributes some sulfur. Despite these low concentrations, sulfur must be further suppressed. Lehtoranta et al. [21] demonstrated the effectiveness of a sulfur trap installed upstream of the MOC, protecting it from sulfur poisoning.

Another technical challenge facing MOCs is their high light-off temperature (LOT), which is typically around 400 °C for methane [22]. Catalyst regeneration may require in excess of 500–700 °C [23], [24], which is considerably higher than other catalytic systems like diesel oxidation catalysts (DOC) or selective catalytic reduction (SCR), which operate at around 160–220 °C [25], [26]. A high LOT necessitates more energy to maintain effective catalyst conversion efficiency. Conversion efficiency suffers significantly when the catalyst temperature drops below this threshold. Consequently, exhaust thermal management (ETM) becomes essential to ensure the exhaust gas temperature (EGT) remains above the required levels across all engine operating conditions.

Conventional ETM techniques, such as post-injection, have been widely used to increase EGT without requiring hardware modifications [27]. Other approaches, including intake/exhaust throttling, offer improved EGT control with minimal hardware changes [28]. However, these methods often incur a fuel efficiency penalty due to additional fuel injection and reduced gas-exchange efficiency. In contrast, variable valve actuation (VVA) strategies can emulate throttling effects while minimizing the associated efficiency losses [29].

Joshi et al. [30] investigated second exhaust valve opening (2EVO) during the intake stroke, which increased EGT by over 50 °C with only a 3% rise in brake specific fuel consumption (BSFC). Vos et al. [31] studied cylinder deactivation (CDA), achieving EGT gains exceeding 100 °C and even fuel savings of 1.5%. Kim et al. [29] conducted comprehensive numerical studies using predictive combustion and emissions models, concluding that CDA was the most fuel-efficient VVA strategy. It increased EGT by over 200 °C while improving fuel efficiency by up to 2.5%. Intake modulation strategies, such as early or late intake valve closing, also showed promising results, with EGT increases of up to 150 °C and moderate BSFC penalties (<5%). Exhaust modulation strategies, including early or late exhaust valve closing, were found to be the least efficient, yielding small EGT increases (<100 °C) and high fuel penalties (>15%). A detailed analysis of VVA's role in ETM can be found in the review by Kim et al. [32].

These VVA strategies demonstrate significant potential for efficient ETM, but most studies to date have been conducted on small-scale, on-road or off-road compression ignition (CI) engines using conventional diesel. In contrast, large-bore marine engines, either conventional DF or RCCI, have distinct combustion characteristics. Notably, they have lower peak temperatures and significantly higher thermal inertia, so it remains unclear whether these promising VVA strategies can be directly applied to large marine engines running on NG.

The present study bridges this knowledge gap by conducting a numerical investigation of two selected VVA strategies and lambda control via wastegate actuation, assessing their viability for efficient ETM in a state-of-the-art, large-bore, medium-speed, RCCI marine engine. The simulations were carried out using the commercial one-dimensional (1D) engine modeling toolchain GT-Suite, leveraging a well-validated engine model to provide insights into how VVA and lambda control can support thermal management in an RCCI marine engine.

Methodology

Experimental setup

A validated GT-Power model of a prototype RCCI research engine forms the cornerstone of this study's simulation framework. The model is calibrated and verified using high-fidelity experimental data acquired from the Wärtsilä 6L20 research engine. This is derived from the Wärtsilä 20 series and tailored for advanced dual-fuel investigations. All the research engine components, except the crankshaft and connecting rods, have been modified to maximize research flexibility and facilitate rapid integration of new technologies. Table 1 summarizes the key specifications of the engine during the test campaign. The engine features an inline six-cylinder configuration with a fully variable electrohydraulic valve actuation system (EHVA), which provides complete freedom in adjusting both valve timing and lift. Air charging, as illustrated in Figure 1, is achieved via a two-stage turbocharging system arranged in series, comprising a low-pressure (LP) and high-pressure (HP) compressor and turbine. This configuration is further enhanced by the integration of two wastegates, one dedicated to the high-pressure turbine and the other to the low-pressure turbine. Notably, under most operating conditions, the regulation of boost pressure is predominantly managed by the high-pressure turbine wastegate. The low-pressure wastegate remains closed in the considered experimental campaign. Figure 1 shows the engine airpath and instrumentation. The dashed box indicates the future after-treatment location. Temperature sensor T5 and pressure sensor P5, located immediately upstream of the HP turbine, were used for model validation. Temperature sensor T6, installed just downstream of the LP turbine, provides the exhaust-gas-temperature (EGT) target for this study.

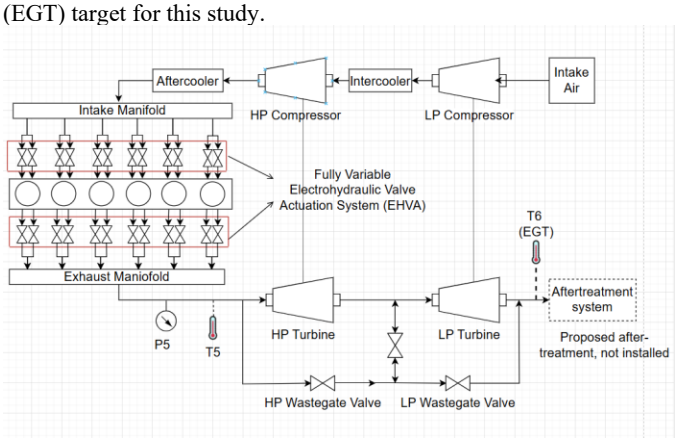

Figure 1: Wärtsilä 6L20 RCCI research engine; airpath schematic with sensor locations and wastegate system. Thin red rectangles outline the fully variable electro-hydraulic valve actuation system (EHVA) that is installed. The black dashed box indicates the proposed after-treatment position (not installed).

High-frequency in-cylinder pressure measurements were recorded with a resolution of 0.2° crank angle over 300 consecutive cycles at each steady-state operating point. These high-resolution data enable accurate derivation of combustion parameters, such as indicated mean effective pressure (IMEP), and heat release rate. Complementary low-frequency measurements include fuel consumption (via Coriolis flow meters for natural gas, and gravimetric methods for light fuel oil (LFO)), intake and exhaust pressures and temperatures, and detailed thermal properties of main engine components.

A central single-needle injector handles the direct injection of high-reactivity LFO, while a low-pressure, multipoint gas injection system upstream of the intake valves delivers natural gas with a methane number of approximately 80. This dual-fuel configuration is designed to operate in reactivity-controlled compression ignition (RCCI) mode, highly relevant to our research objectives.

Table 1: Specifications of the Wärtsilä 6L20 research engine for model calibration and validation

Parameter	Specification
Displacement / Nominal speed	8.80 L / 1000 rpm
Stroke/bore ratio	1.4:1
Air management system	Two-stage turbocharged (in series)
High-reactivity fuel system	Multi-pulse, common-rail direct injection
Low-reactivity fuel system	Low-pressure, multipoint injection upstream of intake valves
Valvetrain	four valves per cylinder; fully variable camless valvetrain via EHVA
Emission system	Horiba Mexa-One (NOx, CO, THC, CO_2, O_2); AVL415S (FSN-Soot)
Indicative system	AVL Indicom; Kistler 6124A pressure transducer (300 bar, 30 pC/bar)
Engine control system	Speedgoat / CANape rapid control prototyping platform
Test fuels	ISO 8217 compliant LFO / natural gas (MN ≈ 80)

Simulation model setup

A model-based investigation was carried out using a one-dimensional (1D) engine simulation, initially developed by the Wärtsilä advanced concept team with the 1D software GT-Suite. Depicted in Figure 2, this comprehensive model incorporates the entire engine system, including intake and exhaust pathways, turbochargers, cylinders, and associated control and mechanical subsystems.

Because the research engine currently operates without an EATS, no exhaust after-treatment module is included in the simulation model. This study was specifically designed to manipulate EGT and control strategies upstream of that point, so modeling the after-treatment would not affect the relative trends while adding unnecessary computational burden.

Overall, the model includes 160 individually parameterized flow components (pipes, flow splits). The geometrical parametrization of the flow components (lengths, diameters, bends, contractions, etc.) and their material specification closely match that of a real engine because they are relevant from the perspective of frictional losses and heat transfer. Note that the wall temperature of the components on the intake side is imposed to match the typical operating temperature. On the exhaust side, however, the pipe wall temperature is dynamically calculated, acknowledging large variability between individual operating conditions. The model is discretized to capture airpath pulsation, using the internal discretization length of 80 mm and 110 mm on the intake and exhaust side, respectively. This gives 279 individual flow volumes, solved using an explicit solver (Runge-Kutta method) [33]with an average timestep of 0.11 ms.

The model incorporates a two-stage turbocharger system, comprising mechanically coupled LP and HP compressors and turbines, corresponding to the experimental setup. Compressor and turbine elements are modeled using a map-based approach. Subsequently, mass multiplier and efficiency multiplier calibration factors were implemented for each compressor and turbine. These factors were strategically employed later in the model development process for the overall calibration of the complete engine model. Wastegate functionality was simulated using a bypass configuration, rather than GT-Power's integrated wastegate feature within the turbine object. This bypass system employed dedicated throttle valves for each turbine stage to control wastegate actuation. This approach was chosen for its enhanced representation of the real turbocharger system.

The study adopted an imposed burn rate profile as its combustion model. This choice was necessitated by the limited availability of dedicated combustion models for dual-fuel/RCCI strategies in GT-Power at the time of research. Moreover, a detailed combustion characterization was not the primary research objective. This approach was deemed appropriate as the investigation centered on broader engine performance metrics rather than in-cylinder combustion phenomena. The burn rate profiles for baseline operating conditions were derived from a three-pressure analysis (TPA) [34]. This TPA model utilized measured in-cylinder pressure and port pressure data to extract representative burn rate profiles for each operating point. It is important to note that the inherent limitations of this imposed burn rate model will be duly considered in the interpretation of the simulation results.

The engine model incorporates two distinct control systems. First, a proportional integral derivative (PID) controller manages boost pressure, modulating the HP wastegate valve at each operating point to achieve the target boost pressure. Second, a brake mean effective pressure (BMEP) controller, functionally similar to a PID algorithm, regulates fuel injection to align the simulated engine's BMEP with experimentally measured values. This BMEP control strategy ensures realistic load representation within the simulation, allowing an accurate assessment of engine performance under defined operating conditions. The aim was to see how different strategies affect the engine if they are supposed to deliver the same load as the base cases. The BMEP controller governs both port-injected natural gas and pilot-injected diesel fuel quantities, preserving their experimentally determined ratio.

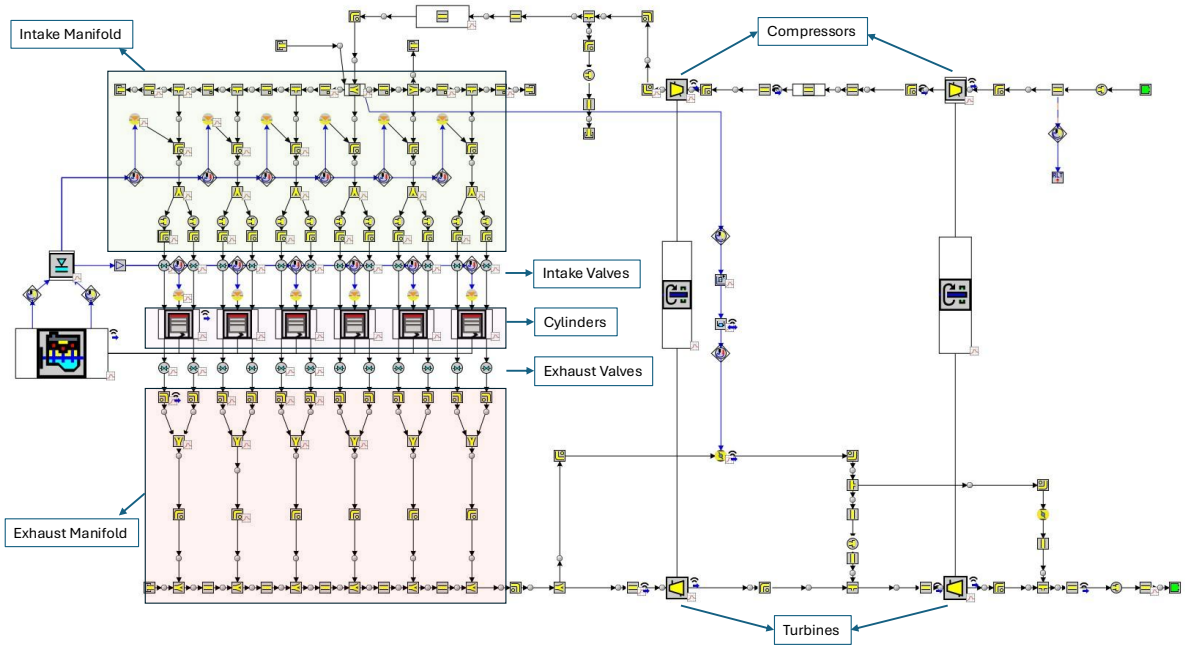

Figure 2: Schematic of the one-dimensional (1-D) engine simulation model developed in GT-Suite.

Simulation conditions

Steady-state simulations were conducted at two selected operating points from the experimental dataset, representing low-load (LL) and medium-load (ML) conditions. These correspond to RCCI operation at 20% and 50% engine load, respectively. Table 2 summarizes the data about these baseline operating points. At each load, the model was first run with the baseline valve timing, defined here as the OEM reference timing used for standard RCCI operation on this engine, prior to any optimization shifts in IVC, EVO, etc. This timing set provides the zero reference for all subsequent ΔCAD sweeps and thus establishes the foundation for analyzing the effectiveness of different EGT strategies. The selection of these load points was motivated by the prevalence of EGT inefficiency at low to medium engine loads. Based on the literature review, three strategies were evaluated:

1. Early exhaust valve opening (EEVO)
2. Early intake valve closing (EIVC)
3. Wastegate lambda control through boost pressure control

Table 2: Key experiment conditions for baseline operating points at low load and medium load

Parameters/Operating point	LL	ML
BMEP	20%	50%
T Intake manifold [°C]	Ref + 14	Ref + 7
P Intake manifold [bar]	Ref + 0.36	Ref + 1.98
Lambda	Ref + 0.013	Ref + 0.24
IVC [°CA]	Ref - 40	Ref - 21
EVO [°CA]	Ref -10	Ref -10
Valve overlap	Negative	Negative
* Ref is the 20% reference point on the conventional dual-fuel version of the experimental engine [35]		

Between five and seven distinct variations were simulated for each of the three strategies. Considerations of both the practical applicability and the operational feasibility of each strategy guided the selection of these variation ranges. Furthermore, the incremental steps within each range were carefully chosen to ensure the capture of potential non-linear behavior across the investigated parameter space.

The first strategy investigated was EEVO, designed to modify the blowdown phase and influence EGT. Figure 3 shows the EEVO profiles for the medium-load (ML) point; the corresponding low-load (LL) profiles are analogous but exhibit a different valve-open duration and are therefore omitted for brevity. Simulations were conducted at both LL and ML, with the exhaust-valve opening (EVO) advanced in 10 °CA steps. Six EEVO settings in addition to the baseline were examined, covering advancements from 10 °CA to 60 °CA relative to the baseline.

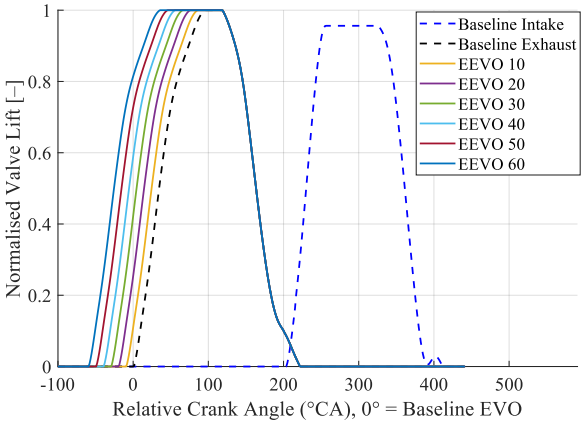

Figure 3: Normalized EEVO valve-lift profiles at ML. Crank-angle axis is relative to the baseline exhaust-valve opening (0° = baseline EVO).

The second strategy explored was EIVC, which focuses on altering the intake stroke characteristics. Figure 4 presents the EIVC profiles at ML; the LL traces follow the same phasing pattern but with a different

duration. For both load points, the intake-valve closing (IVC) was advanced from the baseline in 10 °CA increments. Four EIVC settings plus the baseline were simulated, corresponding to IVC advancements of 10 °CA to 40 °CA.

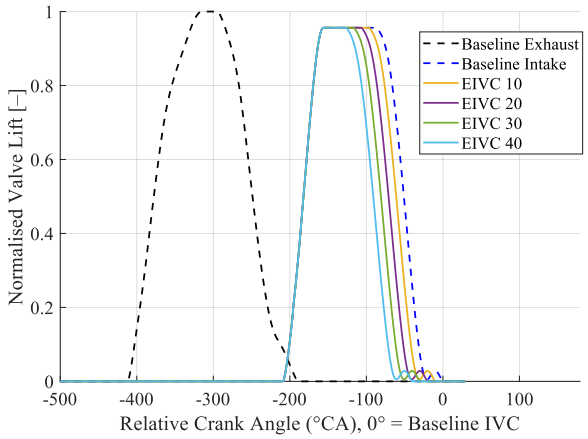

Figure 4: Normalized EIVC valve-lift profiles at ML. Crank-angle axis is relative to the baseline intake-valve closing (0° = baseline IVC).

The third strategy involved wastegate lambda control, achieved through the manipulation of boost pressure. As presented in Table 3, this strategy varied the target boost pressure (p3) relative to the baseline boost pressure for each load condition. Four distinct boost pressure variations, in addition to the baseline, were simulated for both LL and ML operating points. These variations represent stepwise reductions in boost pressure, with each step reducing the target boost pressure by 0.1 bar, giving a total boost pressure reduction range from 0.1 bar to 0.4 bar below the baseline boost pressure for each load. This pressure modulation was realized in the simulation by adjusting the opening of the HP turbine wastegate valve. Controlling the wastegate allows effective management of the exhaust flow through the HP turbine, and consequently the compressor speed and boost pressure, thus influencing both engine airflow and lambda.

Table 3: Simulation parameters for wastegate lambda control strategy (boost pressure difference from baseline)

Load Point	Load (%)	Boost Pressure Difference from Baseline (bar)				
		Test 1	Test 2	Test 3	Test 4	Test 5 (base)
LL	21.4	-0.4	-0.3	-0.2	-0.1	0
ML	50.2	-0.4	-0.3	-0.2	-0.1	0

Results and discussion

Model validation (airpath)

A comprehensive validation process was conducted to ensure the reliability of the one-dimensional engine model for investigating exhaust thermal management strategies. The model's predictive capability was assessed by comparing simulation results against experimental data obtained from the baseline engine configuration at two operating points: LL and ML. These operating points, detailed in Table 2, represent the baseline conditions before the application of VVA and boost control strategies.

The selection of validation parameters was guided by their relevance to the study's objectives and sensitivity to model accuracy, particularly within the airpath and combustion domains. The parameters included: brake-specific fuel consumption (BSFC) as a measure of engine efficiency; air mass flow rate for volumetric efficiency assessment; peak cylinder pressure (Pmax) and crank angle of 50% mass fraction burned (CA50) to evaluate combustion phasing; exhaust pressure before HP turbine (P5) to validate conditions on the exhaust side upstream of the turbocharger; and EGT before exhaust aftertreatment systems (T6) to assess thermal predictions.

Figure 5 illustrates the absolute percentage errors for each selected parameter, alongside established error margins of ±5% for general engine performance parameters and ±2 CAD (°CA) for CA50. Most of the selected parameters exhibit percentage errors within the target ±5% range for both LL and ML conditions. The air mass flow rate shows a slightly higher error at ML, and EGT exhibits a larger error at LL, but all other parameters are well within the acceptable error limits. The CA50 error, notably, remains minimal at both operating points. Given the utilization of an imposed burn rate model, this close agreement in combustion phasing is anticipated, because the model directly dictates the heat release profile timing. The deviations observed for air mass flow rate and temperature after the LP turbine may be attributed to minor model simplifications or experimental uncertainties, inherent in complex engine simulations and measurements. Despite these minor discrepancies, it is crucial to recognize that the study's primary objective is to investigate the trends and relative changes in EGT and efficiency resulting from VVA and lambda control strategies, rather than absolute predictive accuracy under all conditions. Therefore, while absolute accuracy is valuable, the model's ability to capture the direction and magnitude of changes in key parameters due to strategic modifications is paramount.

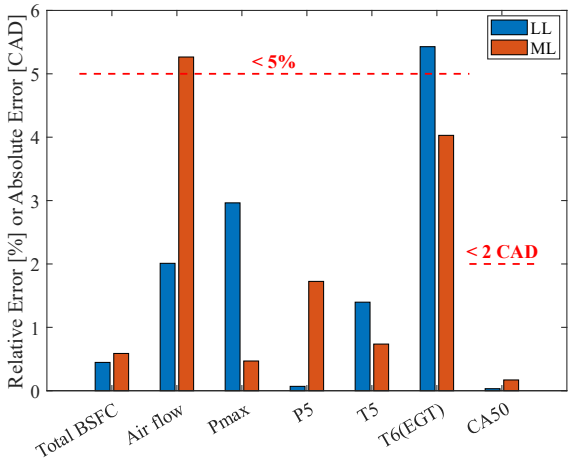

Figure 5: Errors for key performance parameters at low-load (LL) and medium-load (ML) conditions, with two thresholds: a 5% relative error for most parameters and a 2° absolute error (crank angle) for CA50 error margin thresholds

Beyond cycle-averaged performance metrics, validation of the model's dynamic behavior is essential. Therefore, in-cylinder pressure traces, which capture the instantaneous pressure variations throughout the engine cycle, were also analyzed to provide this crucial validation. Figure 6 presents a comparative analysis of the normalized in-cylinder pressure traces for both the low-load (LL) and medium-load (ML) operating points. At each load, the simulation closely follows the experimental data, as expected for a model that employs an imposed burn-rate combustion profile.

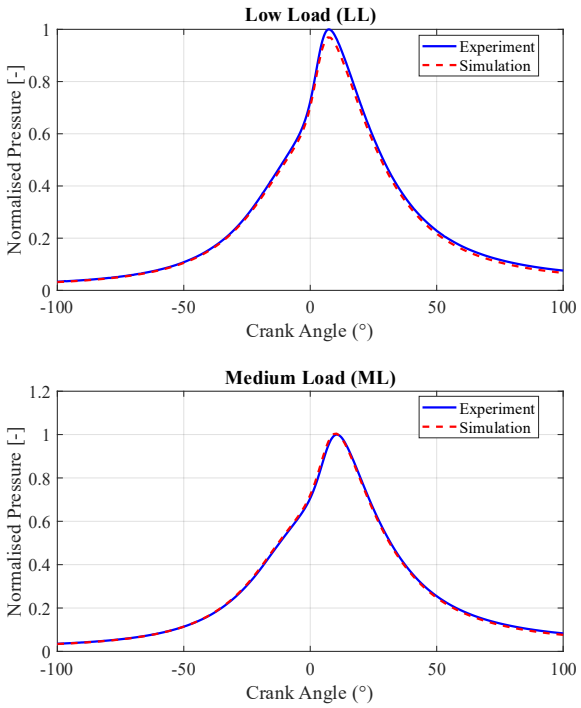

Figure 6: Normalized in-cylinder pressure comparison between simulation and experiment: low-load (top) and medium-load (bottom).

Early exhaust valve opening (EEVO)

The first exhaust thermal management strategy investigated was EEVO. Figure 7 presents the resulting change in EGT, delta exhaust gas temperature (ΔEGT), compared to the baseline case as a function of EEVO advancement (representing the degrees of crank angle by which EVO is advanced from the baseline). There is a clear trend of increasing EGT with greater EEVO advancement for both load points. At LL, advancing EVO by 60°CA results in a ΔEGT of approximately 73 K. A similar trend is observed at ML, although the magnitude of EGT elevation is slightly lower. This EGT increase is attributed to the fundamental mechanism of EEVO: opening the exhaust valve earlier shortens the expansion stroke, leading to less work extracted from the in-cylinder gases and a greater proportion of thermal energy being rejected into the exhaust stream. Furthermore, the fixed boost pressure control in the simulation contributes to EGT elevation. As EEVO is advanced, the higher temperature exhaust gas entering the turbine stage tends to increase boost pressure. To maintain the target boost, the HP wastegate valve opens further, bypassing a larger fraction of hotter exhaust gas directly to the intake of the LP turbine (bypassing the HP turbine). This increased wastegate flow, carrying higher temperature exhaust gas, further contributes to the overall rise in EGT. Thus, EEVO elevates EGT through both reduced expansion work and increased wastegate bypass of hotter exhaust gas.

However, this EGT enhancement is achieved at the expense of engine efficiency. Figure 8 depicts the delta brake thermal efficiency (ΔBTE) trend as a function of EEVO advancement. It shows a monotonic decrease in BTE with increasing EEVO advancement for both LL and ML conditions. For instance, at LL, the BTE reduces from the baseline value by approximately 3.85 percentage points when EVO is advanced by 60°CA. This efficiency penalty is a direct consequence of the shortened expansion stroke in the engine cycle. With an earlier exhaust valve opening, less expansion work is extracted, reducing the overall indicated work. The fuel injection rate must be increased to maintain the BMEP and thus load output, resulting in lower brake thermal efficiency.

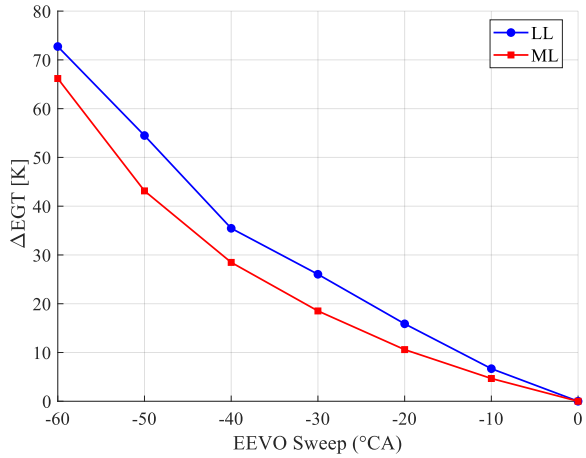

Figure 7: ΔEGT as a function of early exhaust valve opening (EEVO) advancement

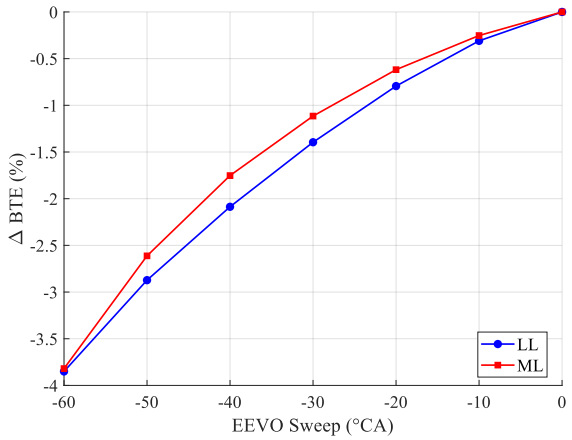

Figure 8: ΔBTE as a function of EEVO advancement

It is important to note that the compression and combustion phases are not substantially altered in the model by this strategy. This is because the primary effect of EEVO occurs during the expansion stroke, after the main combustion event, and with both intake valve timing and boost pressure held constant. Kim et al. [29] also observed the same behavior over various EEVO strategies using a predictive combustion model. Consequently, the imposed burn rate combustion model is deemed sufficiently representative for capturing the dominant thermodynamic effects of EEVO on EGT and efficiency, despite not reflecting potential subtle combustion changes that might occur in a real engine.

Early intake valve closing (EIVC)

The second exhaust thermal management strategy evaluated was EIVC. Simulations were performed at LL and ML conditions, advancing the intake valve closing timing from the baseline, as detailed in Figure 4. Figure 9 illustrates the resulting ΔEGT as a function of EIVC advancement from the baseline. It shows that EIVC effectively elevates EGT across both load conditions. A maximum ΔEGT of approximately 120 °C is achieved at ML with an EIVC advancement of roughly 40°CA. There is a similar trend, albeit with a slightly lower magnitude, observed at LL. This EGT elevation is primarily attributed to the reduction of in-cylinder air mass and the consequential decrease in heat capacity.

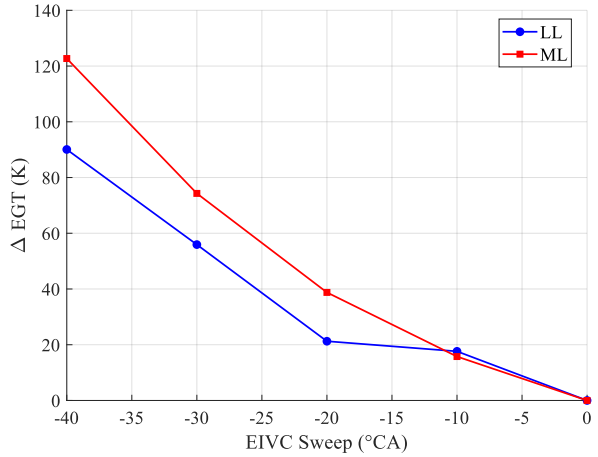

Figure 9: ΔEGT as a function of EIVC advancement

To quantify this reduction in air mass, Figure 10 plots the normalized intake-air flow against EIVC advance. For both load points the flow decreases steadily as the valve closes earlier. An exception occurs at low load: the curves for –10 °CA and –20 °CA almost overlap, because the intake valve closes in a region where IVC timing shifts have little influence on trapped mass; their airflow and EGT responses are therefore nearly identical. In general, shortening the intake duration at constant boost reduces the trapped air mass, and with less mass in the cylinder, the same heat release produces a larger temperature rise. This reduced heat capacity explains the overall elevation in EGT.

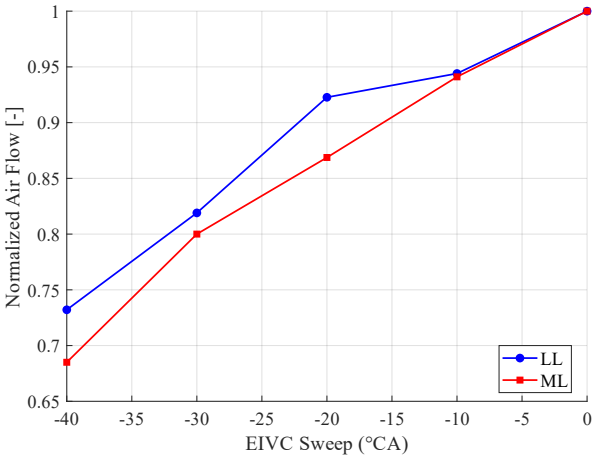

Figure 10: Normalized air flow as a function of EIVC advancement

Figure 11 visualizes the impact on in-cylinder temperature profiles. It presents normalized instantaneous cylinder temperature traces for ML across different EIVC timings. The in-cylinder temperature during the combustion and expansion strokes is noticeably elevated with increasing EIVC advancement. This reinforces the heat capacity reduction mechanism, where less air mass leads to a higher average temperature throughout the cycle, resulting in higher EGT.

Figure 12 shows ΔBTE as a function of EIVC advance and reveals a non-monotonic trend at both load points. At LL, ΔBTE first drops to about –0.1% at a 10 °CA advance, rises slightly at –20 °CA, and then declines again to roughly –0.13% at a 40 °CA advance. This local dip at –10 °CA reflects a shift in the loss balance: the limited gain in pumping efficiency at that timing no longer offsets the rise in heat and exhaust losses. At ML, ΔBTE increases more strongly, peaking at about +0.6% near a 30 °CA advance before tapering to 0.4% at 40 °CA. This complex BTE behavior suggests a nuanced interplay of factors in response to EIVC. The model captures these general trends, but it is important to consider that the inherent limitations of the imposed burn rate combustion model, particularly its inability to fully represent combustion phasing effects, influence the precise magnitude and nature of the predicted BTE variations.

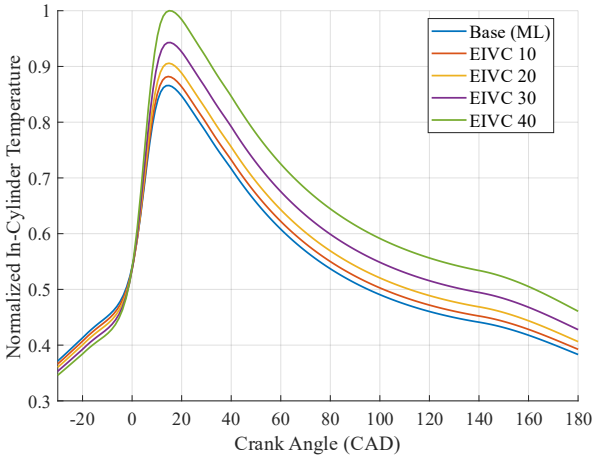

Figure 11: Normalized instantaneous in-cylinder temperature for various EIVC advancements at ML

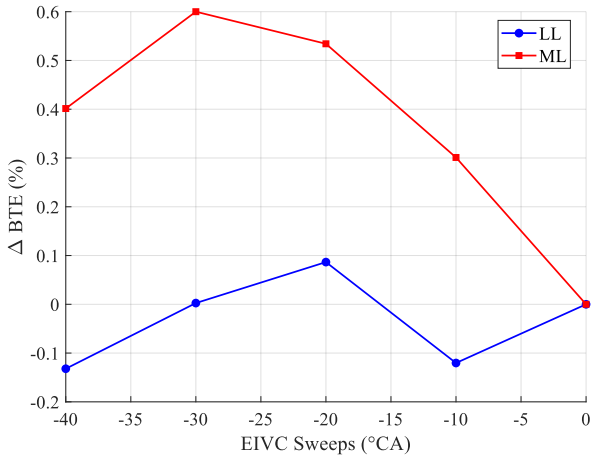

Figure 12: ΔBTE as a function of EIVC advancement

In practice, EIVC initiates multiple interacting effects whose combined influence dictates its net impact on engine efficiency and operation. Primarily, EIVC lowers the effective compression ratio, reducing end-of-compression temperature [36]. This typically delays ignition and retards combustion phasing, which can negatively affect thermal efficiency. Simultaneously, however, EIVC reduces pumping work, particularly at part loads, providing a direct fuel efficiency benefit [37]. Furthermore, under constant boost conditions, EIVC can decrease the trapped air mass, resulting in a lower air-fuel ratio and a richer mixture. This richer mixture may increase combustion temperatures, thereby accelerating the combustion rate and shortening its duration, potentially improving efficiency, despite the later start. This acceleration, however, also increases knock propensity, potentially limiting the practical application of EIVC. Therefore, the actual outcome of implementing EIVC is highly sensitive to the specific engine operating condition and to the interplay with other control strategies that are applied simultaneously, such as injection timing and boost pressure.

Wastegate lambda control

The third exhaust thermal management strategy investigated employs wastegate modulation to control in-cylinder lambda, thereby influencing EGT. This strategy leverages the principle that reducing boost pressure decreases in-cylinder air mass, leading to a relatively richer air-fuel mixture compared to the baseline, but while still maintaining overall lean combustion. As outlined in Table 3, simulations were conducted at low-load (LL) and medium-load (ML) conditions, varying the boost pressure relative to the baseline.

Figure 13 presents the ΔEGT as a function of boost pressure difference, showing the deviation in boost pressure from its baseline. It is evident that reducing boost pressure effectively elevates EGT across both load points., Reducing boost pressure by approximately 0.4 bar at LL yields a ΔEGT of roughly 90 K. There is a similar trend observed at ML, albeit with a lower magnitude of EGT elevation (50 K). This EGT increase is achieved through a combination of two primary mechanisms: reduced in-cylinder air mass (heat capacity) and increased wastegated gas portion, which is similar to the behavior observed in EIVC.

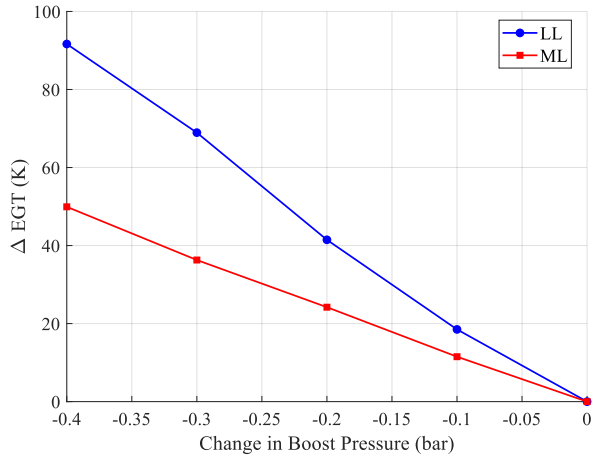

Figure 13: ΔEGT as a function of boost pressure difference for the wastegate lambda control strategy

Figure 14 quantifies the reduction in air mass. It presents the normalized air flow as a function of boost pressure difference, confirming that reducing boost pressure leads to a decrease in normalized air flow rate for both load conditions. This reduced air mass flow contributes to EGT elevation by decreasing the in-cylinder heat capacity.

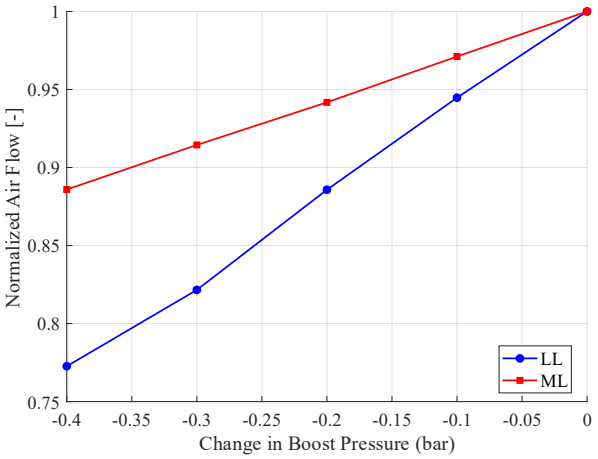

Figure 14: Normalized air flow as a function of boost pressure difference

Figure 15 illustrates how the HP wastegate valve opening deviates from the baseline, as a function of boost pressure difference. It shows that as boost pressure is reduced from the baseline (negative x-axis values), the HP wastegate valve opening angle increases compared with the baseline. The wastegate is modulated towards a more open position when less boost is demanded to achieve lower lambda. This directs a smaller proportion of exhaust gas through the HP turbine, thus reducing the turbine work output and consequently the compressor power on the intake side. This bypassed exhaust gas, having not expanded and cooled within the HP turbine, retains a higher thermal energy. Consequently, the increased portion of wastegated gas contributes to the overall elevation of EGT.

This effect is more pronounced at LL, where achieving the same 0.4 bar reduction in boost requires a larger wastegate opening than at ML. As a result, LL exhibits a stronger response in exhaust-gas temperature: the same pressure decrease yields ΔEGT of 91.5 K at LL versus 50 K at ML. This pronounced load-dependent sensitivity in EGT response is unique compared with the EEVO and EIVC strategies, where both loads exhibit similar behavior, and underlines the particular effectiveness of wastegate control at low load.

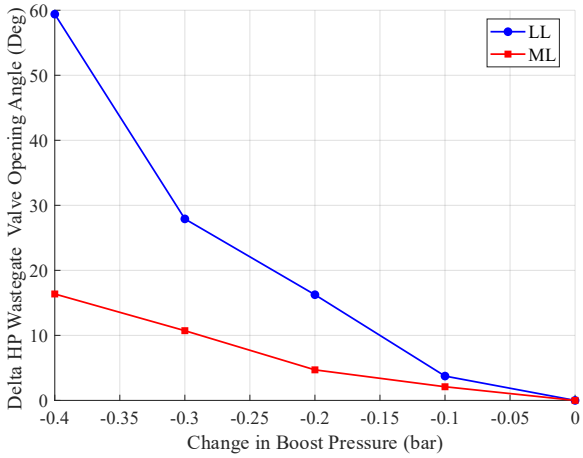

Figure 15: HP wastegate valve opening deviation from baseline as a function of boost pressure

Figure 16 depicts the ΔBTE as a function of boost pressure difference, revealing a non-monotonic trend in ΔBTE across both load conditions. At LL, ΔBTE generally decreases with boost pressure reduction, reaching a minimal decrease of approximately -0.28% at a 0.4 bar boost reduction. Conversely, at ML, ΔBTE exhibits an initial increase, reaching a peak improvement of approximately +0.13% with a boost pressure reduction of around 0.3 bar, before gradually decreasing to approximately +0.12% at a boost reduction of 0.4 bar. These simulated BTE trends suggest a mixed efficiency impact, but once again it is important to bear in mind the inherent limitations of the imposed burn rate combustion model, which does not fully capture potential combustion phasing effects associated with changes in mixture lambda.

Reducing boost pressure to control lambda lowers the trapped air mass, resulting in a richer air-fuel mixture. While this may decrease end-of-compression temperatures, and thus retard combustion initiation due to longer ignition delays, the dominant effect arises during combustion. Similar to effects observed with EIVC, but often more pronounced, the lower lambda significantly increases combustion temperatures. This accelerates the combustion rate and shortens its duration, potentially improving thermal efficiency, despite the delayed start. However, these elevated combustion temperatures severely increase knock propensity and raise oxides of nitrogen (NOx) emissions. Although lower boost pressure also reduces pumping mean effective pressure (PMEP), offering a minor efficiency benefit, the overall viability is primarily determined by the trade-off between

combustion characteristics (phasing, duration) and the critical limitations imposed by knock and NOx.

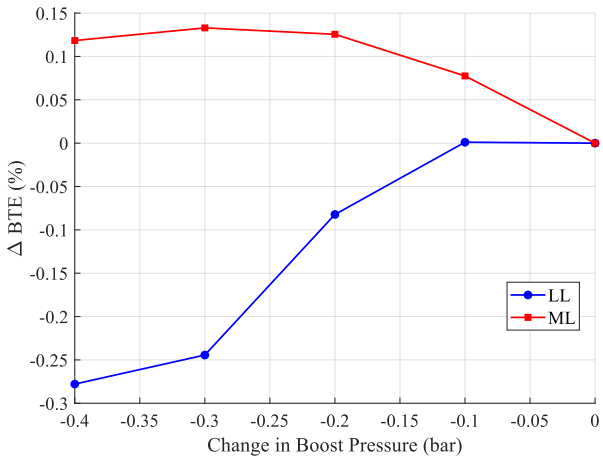

Figure 16: ΔBTE as a function of boost pressure difference

Discussion

Table 4 summarizes the results of the simulations. All three strategies – EEVO, EIVC, and wastegate lambda control – effectively elevate EGT. However, they exhibit varying degrees of effectiveness and efficiency trade-offs. EIVC demonstrates the highest EGT enhancement, reaching a maximum ΔEGT of 122.7 K at ML and 90 K at LL. Wastegate lambda control achieves a ΔEGT of 91.5 K at LL and 50 K at ML. EEVO provides a more moderate EGT increase, with 73 K at LL and 66 K at ML. An important point is that the absolute ΔEGT depends on the back-pressure imposed by an EATS. In an initial sensitivity run with added back-pressure, we observed that increasing back-pressure raised the ΔEGT for all strategies while preserving their relative ranking. To maintain consistency with the experimental configuration, no additional back-pressure was applied in the present simulations.

Turning to brake thermal efficiency (BTE), EEVO consistently presents the least favorable outcome, incurring a substantial BTE reduction of 3.85%. Wastegate lambda control maintains a near-negligible BTE impact, with a slight increase of +0.12% at ML and a minimal decrease of -0.28% at LL. Notably, EIVC exhibits a nuanced BTE response, yielding a slight BTE improvement of +0.4% at the point of maximum EGT gain at ML, while at LL, the BTE reduction remains minimal at -0.13%. This suggests EIVC offers a more favorable efficiency trade-off than that of both EEVO and wastegate lambda control. However, these BTE trends should be interpreted considering the imposed burn rate model's inability to capture combustion phasing effects.

The practical implementation of these strategies introduces additional challenges which must be considered alongside the simulation results. Specifically:

- EEVO: Excessively advanced EVO will reduce power stroke and engine performance.
- EIVC, lambda control: Excessive application decreases the trapped air mass. This reduction is especially critical at mid-to-high loads, where insufficient air can lead to knocking. Furthermore, the resulting lower lambda significantly increases combustion temperatures. This faster, more intense combustion may reduce total hydrocarbon (THC) emissions, but it also causes a drastic increase in NOx formation, necessitating dedicated mitigation strategies. Additionally, maintaining combustion phasing, particularly with EIVC, often requires increased pilot fuel quantities, which can further harm other emissions.

Thus, careful optimization of the control strategies is essential to achieve a proper balance and minimize efficiency penalties.

Table 4: Comparative assessment of EGT management strategies

Strategy	EGT elevation (max ΔEGT)	Input change for max ΔEGT	BTE change (at max ΔEGT)	Primary mechanism(s)	Model limitations (combustion)
Early exhaust valve opening (EEVO)	73 K (LL), 66 K (ML)	60°CA advancement	-3.85%	Shortened expansion stroke & wastegate bypass	Minimal impact
Early intake valve closing (EIVC)	100 K (LL), 122.7 K (ML)	40°CA advancement	+0.4% (ML), -0.13% (LL)	Reduced heat capacity	Moderate impact
Wastegate lambda control	91.5 K (LL), 50 K (ML)	0.4 bar boost reduction	+0.12% (ML), -0.28% (LL)	Reduced heat capacity & wastegate bypass	Moderate impact

Conclusions and outlook

In the pursuit of maritime decarbonization, this study investigated the effectiveness of three exhaust thermal management (ETM) strategies – EEVO, EIVC, and wastegate lambda control – in elevating EGT to enhance the exhaust aftertreatment system efficiency of an RCCI engine. A validated one-dimensional engine model within GT-Suite was used to conduct numerical simulations across low- and medium-load operating conditions to assess the EGT enhancement potential and associated BTE trade-offs for each strategy. The key findings from this model-based investigation are summarized below:

- All three strategies (EEVO, EIVC, and wastegate lambda control) demonstrated a clear capability to elevate EGT, offering viable pathways for exhaust thermal management in dual-fuel engines.
- EIVC and wastegate lambda control emerged as more effective EGT enhancement techniques, achieving significantly higher ΔEGT compared with EEVO. EIVC exhibited the greatest EGT elevation potential, reaching a maximum ΔEGT of more than 120 K at ML and 90 K at LL. Wastegate lambda control further shows a load-dependent behavior, with LL responding more strongly (ΔEGT ≈ 92 K) than ML (≈ 50 K), underscoring its particular effectiveness at low load.
- EEVO provided a moderate EGT increase, but consistently incurred the most substantial efficiency penalty, reducing BTE by 3.85%.
- EIVC presented a nuanced efficiency response, showing a slight BTE improvement of +0.4% at ML alongside significant EGT elevation, suggesting a potential for efficiency-neutral EGT management under specific

operating conditions, while exhibiting a minimal BTE reduction of -0.13% at LL.

- While the imposed burn rate combustion model effectively captured thermodynamic trends, the predicted BTE values, particularly for EIVC and wastegate lambda control, should be interpreted considering the model's inherent limitations in representing complex combustion phasing effects.
- Further research, incorporating advanced combustion models and experimental validation, is recommended for a comprehensive assessment of these EGT management strategies' implications on real-engine performance, efficiency, and emissions. Specific attention should be given to combustion phasing and characteristics.

Further experimental validation of variable-valve-actuation strategies for RCCI optimization is planned under the Flex-CPT project [38] on a different engine platform with comparable cylinder geometry. In these follow-up investigations, the effects of combustion will be studied both experimentally and by simulation using more predictive models than those employed here. The scope will extend beyond after-treatment thermal management to cover key performance metrics such as brake-thermal efficiency, power output, and regulated emissions.

References

1. "2023 IMO STRATEGY ON REDUCTION OF GHG EMISSIONSFROM SHIPS." Accessed: Dec. 29, 2023. [Online]. Available: https://wwwcdn.imo.org/localresources/en/OurWork/Environment/Documents/annex/MEPC%2080/Annex%2015.pdf
2. "INITIAL IMO STRATEGY ON REDUCTION OF GHG EMISSIONS FROM SHIPS ." Accessed: Dec. 29, 2023. [Online]. Available: https://wwwcdn.imo.org/localresources/en/OurWork/Environment/Documents/Resolution%20MEPC.304%2872%29_E.pdf
3. L. Marchitto, L. De Simio, S. Iannaccone, V. Pennino, and N. Altieri, "Retrofit of a Marine Engine to Dual-Fuel Methane–Diesel: Experimental Analysis of Performance and Exhaust Emission with Continuous and Phased Methane Injection Systems," *Energies (Basel)*, vol. 17, no. 17, Sep. 2024, doi: 10.3390/en17174304.
4. Forster, P., Storelvmo, T., Armour, K., Collins, W. et al., "The Earth's Energy Budget, Climate Feedbacks, and Climate Sensitivity," In *Climate Change 2021: The Physical Science Basis. Contribution of Working Group I to the Sixth Assessment Report of the Intergovernmental Panel on Climate Change*, [Masson-Delmotte, V., Zhai, P., Pirani, A., Connors, S.L. et al. (eds.)], Cambridge University Press, Cambridge, United Kingdom and New York, NY, USA, pp. 923–1054, 2021, doi:10.1017/9781009157896.009.
5. M. V. Jensen, R. F. Cordtz, and J. Schramm, "Numerical analysis of methane slip source distribution in a four-stroke dual-fuel marine engine," *Journal of Marine Science and Technology (Japan)*, vol. 26, no. 2, pp. 606–617, Jun. 2021, doi: 10.1007/s00773-020-00760-3.
6. O. Nsaif, S. Kokjohn, R. Hessel, and A. Dempsey, "Reducing Methane Emissions From Lean Burn Natural Gas Engines With Prechamber Ignited Mixing-Controlled Combustion," *J Eng Gas Turbine Power*, vol. 146, no. 6, Jun. 2024, doi: 10.1115/1.4064454.
7. A. Huonder and D. Olsen, "Methane Emission Reduction Technologies for Natural Gas Engines: A Review," Oct. 01, 2023, *Multidisciplinary Digital Publishing Institute (MDPI)*. doi: 10.3390/en16207054.
8. H. Suokko, "Reduction of Methane Slip Emissions from a Medium Speed Dual Fuel Engine," Master thesis, University of Vaasa, 2024.
9. A. Järvi, "Methane slip reduction in Wärtsilä lean burn gas engines," in *Proceedings of the 26th CIMAC World Congress on Combustion Engines*, 2010.
10. J. Hiltner, A. Loetz, and S. Fiveland, "Unburned Hydrocarbon Emissions from Lean Burn Natural Gas Engines—Sources and Solutions," in *Proceedings of the 28th CIMACWorld congress*, 2016.
11. M. Honkanen *et al.*, "Regeneration of sulfur-poisoned Pd-based catalyst for natural gas oxidation," *J Catal*, vol. 358, pp. 253–265, Feb. 2018, doi: 10.1016/J.JCAT.2017.12.021.
12. R. Burch, F. J. Urbano, and P. K. Loader, "Methane combustion over palladium catalysts: The effect of carbon dioxide and water on activity," *Appl Catal A Gen*, vol. 123, no. 1, pp. 173–184, Mar. 1995, doi: 10.1016/0926-860X(94)00251-7.
13. R. L. Mortensen *et al.*, "Understanding the reversible and irreversible deactivation of methane oxidation catalysts," *Appl Catal B*, vol. 344, May 2024, doi: 10.1016/j.apcatb.2023.123646.
14. D. L. Mowery and R. L. Mccormick, "Deactivation of alumina supported and unsupported PdO methane oxidation catalyst: the effect of water on sulfate poisoning," 2001.
15. X. Li, X. Wang, K. Roy, J. A. Van Bokhoven, and L. Artiglia, "Role of Water on the Structure of Palladium for Complete Oxidation of Methane," *ACS Catal*, vol. 10, no. 10, pp. 5783–5792, May 2020, doi: 10.1021/ACSCATAL.0C01069/SUPPL_FILE/CS0C01069_SI_001.PDF.
16. N. Ottinger, R. Veele, Y. Xi, and Z. G. Liu, "Desulfation of Pd-based Oxidation Catalysts for Lean-burn Natural Gas and Dual-fuel Applications," *SAE Int J Engines*, vol. 8, no. 4, pp. 1472–1477, Apr. 2015, doi: 10.4271/2015-01-0991.
17. J. K. Lampert, M. S. Kazi, and R. J. Farrauto, "Palladium catalyst performance for methane emissions abatement from lean burn natural gas vehicles," *Appl Catal B*, vol. 14, no. 3–4, pp. 211–223, Dec. 1997, doi: 10.1016/S0926-3373(97)00024-6.
18. N. M. Kinnunen, J. T. Hirvi, K. Kallinen, T. Maunula, M. Keenan, and M. Suvanto, "Case study of a modern lean-burn methane combustion catalyst for automotive applications: What are the deactivation and regeneration mechanisms?," *Appl Catal B*, vol. 207, pp. 114–119, Jun. 2017, doi: 10.1016/J.APCATB.2017.02.018.
19. S. Heikkilä *et al.*, "Methane Catalyst Regeneration with Hydrogen Addition," in *Proceedings of the 29th CIMACWorld Congress on Combustion Engine*, 2019.
20. J. M. Jones *et al.*, "Sulphur poisoning and regeneration of precious metal catalysed methane combustion," *Catal Today*, vol. 81, no. 4, pp. 589–601, Jul. 2003, doi: 10.1016/S0920-5861(03)00157-3.
21. K. Lehtoranta, P. Koponen, H. Vesala, K. Kallinen, and T. Maunula, "Performance and regeneration of methane oxidation catalyst for LNG ships," *J Mar Sci Eng*, vol. 9, no. 2, pp. 1–12, Feb. 2021, doi: 10.3390/jmse9020111.
22. M. Stoian *et al.*, "Total oxidation of methane on oxide and mixed oxide ceria-containing catalysts," Apr. 01, 2021, *MDPI*. doi: 10.3390/catal11040427.
23. P. Auvinen *et al.*, "A detailed study on regeneration of SO2 poisoned exhaust gas after-treatment catalysts: In pursuance of high durability and low methane, NH3 and N2O emissions of heavy-duty vehicles," *Fuel*, vol. 291, May 2021, doi: 10.1016/j.fuel.2021.120223.
24. S. Colussi *et al.*, "Nanofaceted Pd-O sites in Pd-Ce surface superstructures: Enhanced activity in catalytic combustion of methane," *Angewandte Chemie - International Edition*, vol. 48, no. 45, pp. 8481–8484, Oct. 2009, doi: 10.1002/anie.200903581.
25. R. Villamaina, I. Nova, E. Tronconi, T. Maunula, and M. Keenan, "Effect of the NH4NO3 Addition on the Low-T NH3-SCR Performances of Individual and Combined Fe- and Cu-Zeolite

Catalysts," *Emission Control Science and Technology*, vol. 5, no. 4, pp. 290–296, 2019, doi: 10.1007/s40825-019-00140-3.
26. S. Stadlbauer, H. Waschl, A. Schilling, and L. Del Re, "DOC Temperature Control for Low Temperature Operating Ranges with Post and Main Injection Actuation," *SAE Technical Papers*, vol. 2, Apr. 2013, doi: 10.4271/2013-01-1580.
27. B. Wu, Z. Jia, Z. guo Li, G. yi Liu, and X. lin Zhong, "Different exhaust temperature management technologies for heavy-duty diesel engines with regard to thermal efficiency," *Appl Therm Eng*, vol. 186, no. December 2020, p. 116495, 2021, doi: 10.1016/j.applthermaleng.2020.116495.
28. M. Laurén, T. Karhu, M. Laivola, J. Ekman, S. Niemi, and K. Spoof-Tuomi, "Different methods to improve the exhaust gas temperature in modern stage V off-road diesel engine over transient emission cycles," *SAE International*, pp. 0–8, 2020.
29. J. Kim, M. Vallinmaki, T. Tuominen, and M. Mikulski, "Variable valve actuation for efficient exhaust thermal management in an off-road diesel engine," *Appl Therm Eng*, vol. 246, Jun. 2024, doi: 10.1016/j.applthermaleng.2024.122940.
30. M. C. Joshi, G. M. Shaver, K. Vos, J. McCarthy, and L. Farrell, "Internal exhaust gas recirculation via reinduction and negative valve overlap for fuel-efficient aftertreatment thermal management at curb idle in a diesel engine," *International Journal of Engine Research*, vol. 23, no. 3, pp. 369–379, 2022, doi: 10.1177/1468087420984590.
31. K. R. Vos, G. M. Shaver, M. C. Joshi, A. K. Ramesh, and J. McCarthy, "Strategies for using valvetrain flexibility instead of exhaust manifold pressure modulation for diesel engine gas exchange and thermal management control," *International Journal of Engine Research*, vol. 22, no. 3, pp. 755–776, 2021, doi: 10.1177/1468087419880634.
32. J. Kim, A. Soleimani, P. Nousiainen, M. Axelsson, and M. Mikulski, "Variable valve actuation (VVA) for next-generation marine and off-road engines: a comprehensive review for meeting future emissions legislation," *Appl Energy*, 2025, *in press.*
33. J. R. Cash and A. H. Karp, "A Variable Order Runge-Kutta Method for Initial Value Problems with Rapidly Varying Right-Hand Sides," *ACM Transactions on Mathematical Software (TOMS)*, vol. 16, no. 3, pp. 201–222, Jan. 1990, doi: 10.1145/79505.79507.
34. K. Goerg and T. Morel, "Use of TPA (Three-Pressure analysis) to obtain burn rates and trapped residuals," in *GT-SUITE Conference*, 2005.
35. Wärtsilä 20DF product guide. Vaasa, Finland, WÄRTSILÄ FINLAND Oy (2024)
36. J. P. Zammit, M. McGhee, P. J. Shayler, T. Law, and I. G. Pegg, "The effects of early inlet valve closing and cylinder disablement on fuel economy and emissions of a direct injection diesel engine," *Energy*, vol. 79, pp. 100–110, Jan. 2015, doi: 10.1016/j.energy.2014.10.065.
37. L. Teodosio, D. Pirrello, F. Berni, V. De Bellis, R. Lanzafame, and A. D'Adamo, "Impact of intake valve strategies on fuel consumption and knock tendency of a spark ignition engine," *Appl Energy*, vol. 216, pp. 91–104, Apr. 2018, doi: 10.1016/j.apenergy.2018.02.032.
38. Flexible Clean propulsion Technologies." Accessed: June. 11, 2025. [Online]. Available: https://cleanpropulsion.org/

Contact Information

Amir Soleimani
University of Vaasa
School of Technology and Innovations
Energy Technology Fabriikki F387, Yliopistonranta 10, 65200 Vaasa, Finland
Amir.soleimani@uwasa.fi
Mobile Phone: +358 29 449 8773

Acknowledgments

The authors wish to explicitly acknowledge that this research was sponsored by Wärtsilä Oy. Amir Soleimani also acknowledges the Otto A. Malm Foundation for a research grant that supported manuscript preparation.

Definitions/Abbreviations

1D	one-dimensional
2EVO	second exhaust valve opening
BMEP	brake mean effective pressure
BSFC	brake specific fuel consumption
BTE	brake thermal efficiency
CA50	crank angle at 50 % mass fraction burned
CDA	cylinder deactivation
C–H	carbon–hydrogen bond
CH_4	methane
CI	compression ignition
CO_2	carbon dioxide
DF	dual-fuel
DOC	diesel oxidation catalyst
EATS	exhaust aftertreatment systems
ECA	emission control area
EEVO	early exhaust valve opening
EGT	exhaust gas temperature
EHVA	electrohydraulic valve actuation system
EIVC	early intake valve closing
ETM	exhaust thermal management
EVO	exhaust valve opening
GHG	greenhouse gas
GWP	global warming potential
GWP20	global warming potential over a 20-year timeframe
HP	high-pressure
IMEP	indicated mean effective pressure
IMO	International Maritime Organization
IVC	intake valve closing
LFO	light fuel oil
LOT	light-off temperature
LP	low-pressure
MOC	methane-oxidation catalyst
NG	natural gas
NOx	nitrogen oxides

p3	boost pressure after the low-pressure compressor
P5	exhaust pressure before the high-pressure turbine
Pd	palladium
PID	proportional–integral–derivative controller
Pmax	peak cylinder pressure
PMEP	pumping mean effective pressure
ppm	parts per million
RCCI	reactivity-controlled compression ignition
SCR	selective catalytic reduction
SO_2	sulfur dioxide
T6	exhaust gas temperature before the exhaust aftertreatment system
THC	total hydrocarbons
TPA	three-pressure analysis
VVA	variable valve actuation
ΔBTE	change in brake thermal efficiency relative to the baseline
ΔEGT	change in exhaust gas temperature relative to the baseline